CHEMISTRY OF MATERIALS

ARTICLE

pubs.acs.org/cm

# Solvent Effects on Morphologies of Mesoporous Silica Spheres Prepared by Pseudomorphic Transformations

Won Cheol Yoo and Andreas Stein*

Department of Chemistry, University of Minnesota, Minneapolis, Minnesota 55455, United States

Supporting Information

**ABSTRACT:** In surfactant-induced, pseudomorphic transformations of submicrometer-sized nonporous spheres to mesoporous silica spheres, the surface morphologies of the products depend on the solvent used during the initial Stöber synthesis. After hydrothermal transformations employing cetyltrimethylammonium bromide (CTAB) as a surfactant, pseudomorphic products of parent silica spheres synthesized in ethanol (HT-$SiO_2$-EtOH) are mesoporous throughout and have smooth surfaces. In contrast, products from spheres synthesized in isopropanol (HT-$SiO_2$-*i*PrOH) or butanol (HT-$SiO_2$-BuOH) possess highly corrugated shells surrounding a nonporous core. On the basis of $^{29}Si$ solid-state magic angle spinning (MAS) NMR spectra, this significant change in surface morphology after the hydrothermal transformation is related to small differences in the degree of condensation of the parent silica spheres. In the case of HT-$SiO_2$-EtOH, the higher degree of condensation of the parent spheres limits sphere dissolution, and the transformation is mostly pseudomorphic. For the other two systems, parent spheres are more reactive and release more silica into solution. Porous shells are therefore formed on the surface of the remaining spheres. Morphological changes were investigated by scanning and transmission electron microscopy. The porosity of the mesoporous silica spheres produced by these reactions was determined by nitrogen sorption measurements and small-angle X-ray scattering. The diffusion depth of CTAB was revealed by nanocasting carbon into the mesoporous silica spheres via phenol-paraformaldehyde gas-phase polymerization and subsequently removing the silica structure. As a result of limited surfactant penetration into the cores of HT-$SiO_2$-*i*PrOH spheres, replicated mesoporous carbon spheres possess a corrugated mesoporous shell and a hollow core.

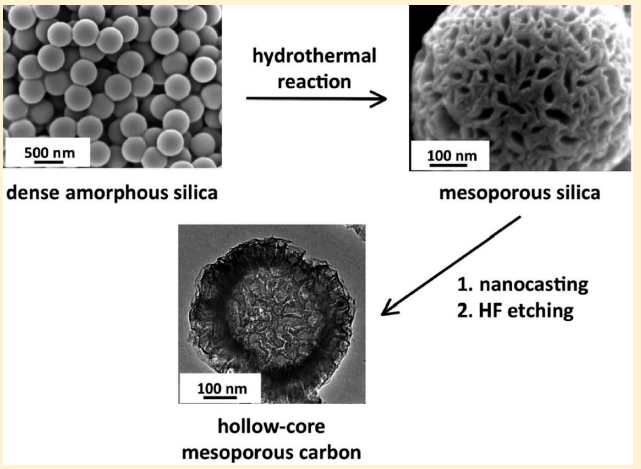


**KEYWORDS:** Stöber synthesis, pseudomorphic transformation, surfactant, mesoporous silica

## 1. INTRODUCTION

Mesoporous silica spheres with controllable pore sizes, narrow pore size distributions, and high surface areas are of interest for various applications including catalysis,[1−3] drug delivery,[4−6] packing materials for chromatography,[7−9] and other applications.[10−15] Several direct methods have been developed to synthesize mesoporous silica spheres using surfactants as templates for mesopores during sphere formation.[10−12,16−22] Some of these approaches produce uniform spheres with well ordered mesopores, but often it is challenging to avoid sphere aggregation and maintain good size control and monodispersity. In the case of amorphous, dense silica spheres, the well-established Stöber method yields products with controllable size, smooth surfaces, and high monodispersity.[23] To build on these structural advantages and also introduce mesoporosity into Stöber spheres, surfactant-induced pseudomorphic transformations have been developed.[24] Pseudomorphic transformations are reactions in which chemical components change, for example, through dissolution and reprecipitation, while the shape of a solid material is preserved. Pseudomorphic transformations involving hydrothermal treatment of dense, amorphous silica spheres provide an alternative method to direct syntheses of mesoporous silica spheres, retaining the sizes and monodispersity of the original silica spheres.[8,24−27]

Here, we investigate the influence of the solvent used in syntheses of dense silica spheres (EtOH, *i*PrOH or BuOH) on the morphology and texture of mesoporous products obtained after pseudomorphic transformations. In particular, we test the hypothesis that the solvent influences the degree of condensation in the parent silica spheres, which then determines the extent of silica dissolution during hydrothermal transformations and the pore architecture of product spheres, both at their surface and in their bulk. Different solvent environments result in slightly different degrees of condensation of amorphous, nonporous silica spheres. However, these small differences produce significant

**Received:** September 30, 2010
**Revised:** February 11, 2011
**Published:** March 04, 2011

changes in surface morphologies following hydrothermal reactions under specific conditions. After hydrothermal transformations employing a long-chain alkylammonium surfactant, pseudomorphic products of parent silica spheres synthesized in EtOH possess smooth surfaces, whereas products from spheres synthesized in *i*PrOH or BuOH possess highly corrugated surfaces. In addition, by using the silica spheres with corrugated surfaces as templates for nanocasting (gas-phase polymerization and carbonization of phenol-paraformaldehyde inside mesoporous silica spheres and subsequent removal of silica with hydrofluoric acid), mesoporous carbon spheres with hollow cores and surface morphologies resembling those of the mesoporous silica spheres are formed. These core−shell structures provide indirect information about the diffusion depth of surfactant molecules into the parent silica spheres during the pseudomorphic transformation and reveal that the cores of the mesoporous silica spheres with corrugated surfaces must have remained solid. Hence, these processes provide new ways to synthesize silica spheres with dense cores and mesoporous shells and hollow carbon spheres with mesoporous shells.

## 2. EXPERIMENTAL SECTION

**Chemicals.** The following chemicals were used without further purification: tetraethyl orthosilicate (TEOS, Aldrich, 98%), ammonium hydroxide (Fisher Scientific, 29.36%), EtOH (Pharmco-AAPER, 99.98%), *i*PrOH (Mallinckrodt, 99.5%), *n*-BuOH (Fisher Scientific, 99.8%), sodium hydroxide (Mallinckrodt, 99%), CTAB (Aldrich), phenol (Fisher Scientific, 99%), paraformaldehyde (Aldrich, 95%), hydrofluoric acid (Mallinckrodt, 48%). Milipore water with a resistivity 18.2 MΩ-cm was used for all reactions.

**Preparation of Silica Spheres.** Silica spheres were synthesized by the Stöber method.[23] Mixtures of 160 mL of EtOH, *i*PrOH, or BuOH with 16 mL of ammonium hydroxide and 7 g of TEOS were stirred at room temperature in a stoppered 500-mL round-bottom flask for 20 h. The silica spheres were recovered and purified by multiple cycles of centrifugation and washing with EtOH. They were dried at 70−80 °C overnight before being used for hydrothermal reactions. The products were denoted $SiO_2$-EtOH, $SiO_2$-*i*PrOH, and $SiO_2$-BuOH, depending on the solvent used.

**Hydrothermal Reactions.** The amorphous parent silica spheres were transformed to mesoporous silica spheres using pseudomorphic transformation reactions. Amorphous silica spheres (0.044 g) dispersed in EtOH (2.53 mL) were added to a mixture of CTAB (0.05 g), water (10 mL), and NaOH (0.013 g) and stirred at room temperature for 30 min. The molar ratio of all components was 1 $SiO_2$: 0.18 CTAB: 0.44 NaOH: 750 $H_2O$: 75 EtOH. The hydrothermal reaction was carried out in a Teflon-lined autoclave at 100 °C for 24 h. The products were recovered and purified by multiple cycles of centrifugation and washing with EtOH. The surfactant was removed from the mesoporous silica spheres by calcination in air at 550 °C for 6 h (heating rate 1 °C/min). The final products were denoted HT-$SiO_2$-EtOH, HT-$SiO_2$-*i*PrOH, and HT-$SiO_2$-BuOH, depending on the solvent used in the Stöber synthesis of the parent spheres.

**Preparation of Hollow-Core@Mesoporous-Shell Carbon Spheres by Nanocasting.** Mesoporous silica spheres (HT-$SiO_2$-*i*PrOH) were used as templates for nanocasting carbon spheres, following a published procedure based on phenol-paraformaldehyde gas-phase polymerization.[28,29] Calcined mesoporous silica spheres (0.044 g HT-$SiO_2$-*i*PrOH or HT-$SiO_2$-EtOH) were stirred for 1 h in a mixture containing 5 mL of EtOH, 5 mL of water, and 0.03 g of $AlCl_3 \cdot H_2O$ to introduce Al into the structure as a polymerization catalyst. The Al-loaded spheres were washed with EtOH, dried at 70−80 °C overnight, and calcined for 4 h at 550 °C (heating rate 1 °C/min). A flask containing phenol (0.05 g), paraformaldehyde (0.035 g), and calcined Al-mesoporous silica spheres (0.044 g) was evacuated under static vacuum (- 70 kPa) for 4 h and then heated at 100 °C for 24 h in a closed system. The color of the material changed from white to dark-red. The phenolic resin inside Al-mesoporous silica spheres was carbonized by heating the sample in nitrogen at 160 °C for 5 h (heating rate 1 °C/min) and then at 850 °C for 7 h (heating rate 5 °C/min). Silica was removed by extraction with hydrofluoric acid (10 wt %) for 24 h. ***Caution!*** *HF is highly corrosive and toxic and must be handled according to procedures specified by the Materials Safety Data Sheet for HF.* The product spheres were labeled PFC-*i*PrOH or PFC-EtOH, depending on the parent spheres.

**Materials Characterization.** Scanning electron microscopy (SEM) images were obtained using a JEOL 6700 microscope with an accelerating voltage of 5 kV and an applied current of 20 mA. All siliceous samples were coated with 5 nm of Pt. Size measurements of the large mesopores/small macropores on the sphere surfaces were based on SEM images using about 30 different pores for each sample and using ImageJ software. Transmission electron microscopy (TEM) images were obtained using a JEOL 1210 microscope with an accelerating voltage of 120 kV. Samples were prepared on TEM Cu grids covered with Formvar carbon film. Nitrogen sorption measurements were carried out at 77 K on a Quantachrome Instruments Autosorb-1 system. Samples were degassed for 24 h at 150 °C. The Brunauer−Emmett−Teller (BET) method was applied to estimate specific surface areas. Pore sizes and volumes were calculated from pore size distribution curves in the adsorption branches of the isotherms. Small-angle X-ray scattering (SAXS) data were obtained using a Rigaku RU-200BVH 2-D SAXS instrument with a 12 kW rotating anode with a Cu source and a Siemens Hi-Star multiwire area detector. The distance between the sample and the detector was 54 cm, the exposure time was 300 s, and the step interval 0.01° 2$\theta$. $^{29}$Si NMR spectra were acquired using a Varian VNMRS spectrometer operating at a $^1$H Larmor frequency of 700 MHz and a temperature of 25 °C. Samples were packed into a 3.2 mm rotor and spun at the magic angle (15 kHz) in a BioMAS Varian triple resonance probe. A single 90° pulse of 5.5 $\mu$s duration was applied to the $^{29}$Si channel followed by $^1$H decoupling (75 kHz) during acquisition. A recycle delay of 45 s was used between scans. Totals of 552, 1024, and 1536 scans were acquired for samples $SiO_2$-EtOH, $SiO_2$-*i*PrOH, and $SiO_2$-BuOH, respectively. To examine the reproducibility of the NMR data, a second set of samples was measured using a 4 mm rotor, magic angle spinning at 10 kHz, and 256 scans. All other parameters were kept the same. Relative peak areas of the $Q^4$, $Q^3$, and (for $SiO_2$-BuOH) $Q^2$ peaks were calculated from the phase-corrected spectra by manual fitting of Gaussian functions to match the observed spectra, using OriginPro (version 8.1) software. A 20-point baseline correction was applied, and peak centers ($Q^2$ = 89, $Q^3$ = 98, and $Q^4$ = 108 ppm) were manually selected. Samples for NMR, SAXS, and nitrogen sorption analyses were prepared by combining multiple batches of materials synthesized under identical conditions.

## 3. RESULTS

The surfaces of the parent silica spheres prepared by Stöber syntheses in different solvents ($SiO_2$-EtOH, $SiO_2$-*i*PrOH, and $SiO_2$-BuOH) were smooth on the SEM scale (Figure 1A, D, and G) and the spheres were virtually nonporous (Supporting Information, Figure S1). After pseudomorphic transformation reactions, the average diameters of the mesoporous product spheres all increased {$SiO_2$-EtOH (436 ± 18 nm), HT-$SiO_2$-EtOH (527 ± 20 nm); $SiO_2$-*i*PrOH (623 ± 37 nm), HT-$SiO_2$-*i*PrOH (730 ± 45 nm); $SiO_2$-BuOH (494 ± 23 nm), HT-$SiO_2$-BuOH (733 ± 40 nm)}. The product spheres were more

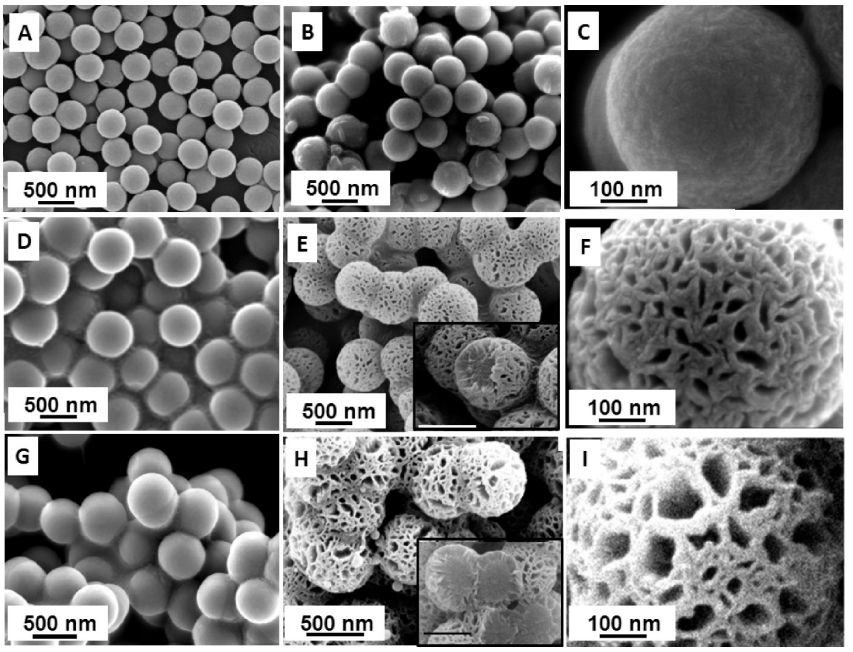


**Figure 1.** SEM images of parent silica and hydrothermal silica spheres: (A) parent silica spheres produced in EtOH ($SiO_2$-EtOH), (B) hydrothermal product HT-$SiO_2$-EtOH, (C) magnified image of HT-$SiO_2$-EtOH, (D) parent silica spheres produced in *i*PrOH ($SiO_2$-*i*PrOH), (E) hydrothermal product HT-$SiO_2$-*i*PrOH and broken structures of HT-$SiO_2$-*i*PrOH in the inset with a scale bar of 500 nm, (F) magnified image of HT-$SiO_2$-*i*PrOH, (G) parent silica spheres produced in BuOH ($SiO_2$-BuOH), (H) hydrothermal product HT-$SiO_2$-BuOH and broken structures of HT-$SiO_2$-*i*PrOH in the inset with a scale bar of 500 nm, (I) magnified image of HT-$SiO_2$-BuOH.

aggregated than the parent spheres. The surface morphologies of the products differed significantly after hydrothermal treatment, depending on the solvent used to synthesize the parent spheres. Smooth surfaces were maintained for HT-$SiO_2$-EtOH silica spheres (Figure 1B and C), which possessed mesoporous channels directed toward the outside surface. These can be observed by TEM in sufficiently thin, near-surface regions (Figure 2A). However, the products from parent silica spheres prepared in *i*PrOH (HT-$SiO_2$-*i*PrOH) or BuOH (HT-$SiO_2$-BuOH) exhibited extensive corrugation with deep cavities at the surface (Figure 1E and F for HT-$SiO_2$-*i*PrOH, and Figure 1H and I for HT-$SiO_2$-BuOH). The openings of most of these cavities were elongated with average dimensions of $37 \pm 17$ nm for the long axis and $16 \pm 6$ nm for the short axis for HT-$SiO_2$-*i*PrOH and dimensions of $60 \pm 20$ nm for the long axis and $31 \pm 13$ nm for the short axis for HT-$SiO_2$-BuOH. Such corrugation has been observed before when mesoporous silica was deposited on denser silica spheres if trimethylbenzene/decane was added to the surfactant system as a cosolvent to expand pores.[30] No such cosolvent was used here. TEM images of HT-$SiO_2$-*i*PrOH and HT-$SiO_2$-BuOH spheres reveal features resembling a mane on the outer part of the spheres (Figure 2B−D). Mesopores in the hydrothermal products HT-$SiO_2$-*i*PrOH and HT-$SiO_2$-BuOH were generally directed radially from the core to the outside, at least near the sphere surfaces. The cores of HT-$SiO_2$-*i*PrOH and HT-$SiO_2$-BuOH spheres appear denser in the TEM images (Figure 2B and 2C), and SEM images of broken spheres reveal a solid-core, corrugated-shell structure (insets in Figure 1E and 1H). In the HT-$SiO_2$-*i*PrOH sample, aggregates of smaller particles were observed (Figure 2B inset) in addition to the larger spheres. These side products are believed to have formed during the hydrothermal transformation by direct surfactant templating

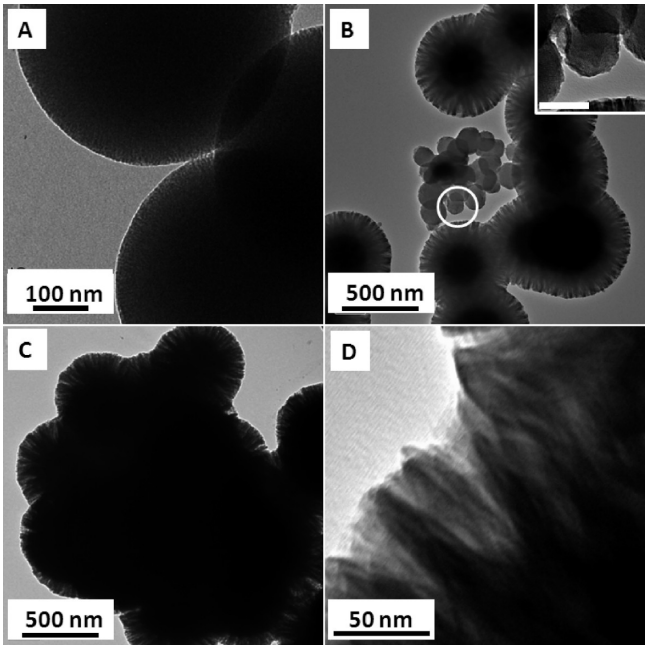


**Figure 2.** TEM images of hydrothermal reaction products (A) HT-$SiO_2$-EtOH, (B) HT-$SiO_2$-*i*PrOH, and (C) HT-$SiO_2$-BuOH. The inset in (B) shows an enlargement of the circled region with a scale bar of 100 nm. (D) shows a higher magnification image of HT-$SiO_2$-*i*PrOH.

of dissolved silica, and they could be removed by multiple centrifugation.

A published diffraction pattern of spherical MCM-41 particles that were synthesized by incorporating CTAB directly in a Stöber synthesis showed a major reflection indexed as (100) and lower-intensity, overlapping (110) and (200) peaks of a hexagonal pore


dx.doi.org/10.1021/cm102829m |*Chem. Mater.* 2011, 23, 1761–1767

system.[31] Those data were interpreted in terms of local hexagonal symmetry around individual mesopores with less long-range order and an overall spherically symmetric pore distribution. The SAXS pattern of HT-$SiO_2$-EtOH resembles this pattern (Figure 3). The (100) and higher order peaks are relatively broad as a result of limited long-range order.[25,32] For HT-$SiO_2$-*i*PrOH the intensity of the (100) peak is significantly reduced and in case of HT-$SiO_2$-BuOH, a (100) peak is missing completely. Because of the corrugated shell of these spheres, mesopores are confined to smaller regions, causing extensive line broadening. In addition, surface corrugation may have perturbed the assembly of surfactant molecules near the surface, reducing the mesopore order. The *d*-spacing values corresponding to the (100) reflections of the hydrothermally treated spheres are listed in Table 1.

To further investigate the density and porosity gradients across the spheres, we synthesized carbon replica structures of HT-$SiO_2$-*i*PrOH and HT-$SiO_2$-EtOH spheres by nanocasting.

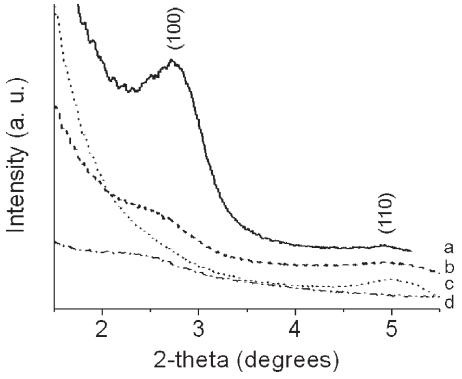


**Figure 3.** SAXS patterns of hydrothermal products and nanocast carbon spheres: (a) HT-$SiO_2$-EtOH, (b) HT-$SiO_2$-*i*PrOH, (c) HT-$SiO_2$-BuOH, and (d) PFC- *i*PrOH.

Nanocasting is an efficient method for producing inverse replica structures of porous materials.[33,34] Structural analysis of the products can be employed to deduce the structure of the template used for nanocasting. After introduction of aluminum into the spheres as a catalyst for polymerization, the spheres were exposed to a gas-phase phenol-paraformaldehyde mixture, which was polymerized and carbonized (Figure 4). Following removal of silica by extraction with hydrofluoric acid, an irregular network of interconnected carbon spheres was recovered from the HT-$SiO_2$-*i*PrOH preforms (Figure 5A and 5B). The average diameter of the carbon spheres (548 ± 27 nm) was lower than that of the silica preform, most likely because of radial contraction during the carbonization process. Some of the spheres were broken, revealing a hollow core, surrounded by about 50−120 nm-thick porous shells, that is, a little thinner than the mesoporous shells in the preforms. The pore cross sections visible by SEM within the shell structures had average dimensions of 34 ± 8 nm for the longer axis and 22 ± 7 nm for the short axis. In TEM images (Figure 5C and 5D) the shell has a mane-like appearance, similar to that observed for the silica preforms. The SAXS pattern for the hollow carbon spheres is also similar to that of the preforms with nearly identical peak positions and widths, albeit lower intensities (Figure 3). The hollow core confirms that polymer could penetrate the preforms only to a limited depth, providing further support for the dense core in the mesoporous silica spheres. In case of the carbon replica from HT-$SiO_2$-EtOH (PFC-EtOH), no hollow spheres were observed and, therefore, mesopores must have extended deeper in HT-$SiO_2$-EtOH, similar to the products from pseudomorphic transformations reported by Martin et al.[24] A TEM image of the surface region of the carbon replica PFC-EtOH revealed worm-like mesopores (Supporting Information, Figure S2).

All three hydrothermal silica products and the carbon replica material (PFC-*i*PrOH) exhibited type IV nitrogen sorption isotherms, typical for capillary condensation in mesopores of

**Table 1. Textural Characteristics of Pseudomorphic Silica Products and Nanocast Carbon Spheres**

| sample | $S_{BET}$ ($m^2\ g^{-1}$) total/micropore[a] | pore volume ($cm^3\ g^{-1}$) total/micropore[a] | pore diameter (nm)[b] | wall thickness (nm)[c] | *d*-spacing (nm)[d] | Δdiameter (nm)[e] | shell thickness (nm)[f] |
|---|---|---|---|---|---|---|---|
| HT-$SiO_2$-EtOH | 729/0 | 0.50/0 | 2.1 | 1.7 | 3.3 | 91 | NA[g] |
| HT-$SiO_2$-*i*PrOH | 124/0 | 0.17/0 | 2.2 | 2.0 | 3.6 | 107 | 113 ± 29 |
| HT-$SiO_2$-BuOH | 219/0 | 0.50/0 | 2.4 | ND[h] | ND[h] | 239 | 151 ± 20 |
| PFC-*i*PrOH[i] | 2100/105 | 2.04/0.05 | 2.3 | 1.3−1.9 | 3.6 | −182 | 50−120 |

[a] The *t*-method was used to estimate micropore surface areas and pore volumes. [b] Pore diameters were estimated from peaks in the pore size distribution curves that were derived from adsorption branches. [c] Wall thicknesses were calculated based on a 2-D hexagonal mesopore geometry (thickness = $d_{100} \times 2/\sqrt{3}$ − pore diameter). Since the pore geometry for PFC-*i*PrOH is not clearly identified by the SAXS pattern, a range is provided, the lower limit being estimated by assuming a worm-like geometry (thickness = $d_{100}$ − pore diameter) and the upper limit by 2-D hexagonal geometry. [d] *d*-spacings of the (100) reflection. [e] This refers to the change in average diameter of product spheres compared to parent spheres. [f] Estimated from SEM or TEM images. [g] Not applicable. [h] Not determined because of the disordered mesoporous structure. [i] Nanocast carbon spheres from HT-$SiO_2$-*i*PrOH mesoporous silica spheres.

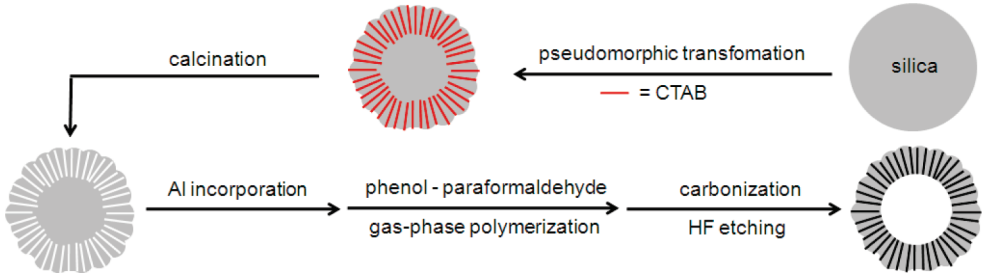


**Figure 4.** Schematic illustration of the preparation of hollow carbon spheres by nanocasting.


dx.doi.org/10.1021/cm102829m |*Chem. Mater.* 2011, 23, 1761–1767

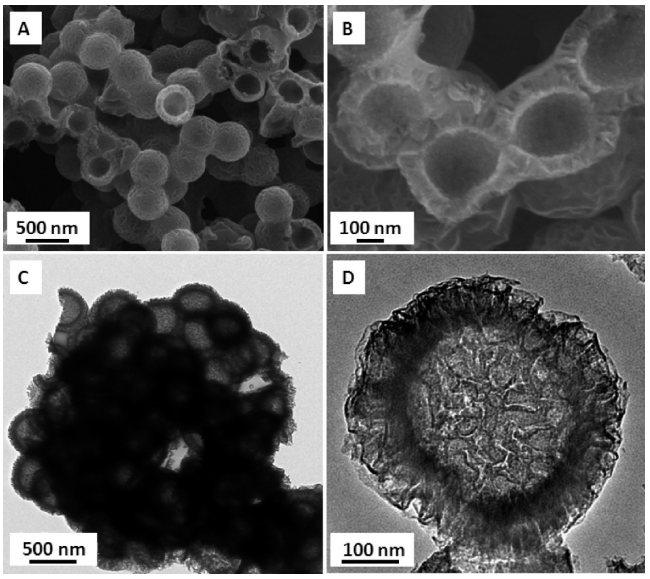


**Figure 5.** SEM (A and B) and TEM (C and D) images of nanocast hollow carbon spheres after HF etching (PFC-*i*PrOH).

MCM-41 type materials (Figure 6). While mesopore diameters and wall thicknesses were similar for all four samples, the specific BET surface areas and pore volumes differed widely (Table 1). The two silica samples with corrugated surfaces (HT-$SiO_2$-*i*PrOH and HT-$SiO_2$-BuOH) had significantly lower specific surface areas than HT-$SiO_2$-EtOH, likely resulting from the denser cores in the former samples. The very high surface area, large pore volume, and presence of additional micropores of PFC-*i*PrOH are often seen in mesoporous carbons prepared by nanocasting methods.

## 4. DISCUSSION

It is notable that the samples obtained in the different preparations had similar pore alignment at the surfaces but vastly different pore textures and surface morphologies. Near the sphere surfaces, the hydrothermal reaction products from silica spheres prepared in all three solvents exhibited radial directionality of mesopores. This directionality may result from the combined effects of individual surfactant molecules aligning on the solid sphere surface to reduce the surface energy and their tendency to assemble into micelles.[35,36] In modified Stöber syntheses of mesoporous silica spheres[37] and in syntheses of silica spheres with solid cores and mesoporous shells,[11,17,30] similar radial orientation of mesopores is also observed and has been attributed to preferred alignment of CTAB micelles normal to a growth interface.[38] However, the gradient structure and surface morphologies of the hydrothermal transformation products depended strongly on the solvent used in the initial synthesis.

What causes these drastic differences in surface morphologies and pore textures? In a study by Kim et al.,[30] some surface corrugation was introduced by employing trimethylbenzene/decane cosolvents as swelling agents during deposition of mesoporous silica on nonporous silica cores. No swelling agents were present in the hydrothermal reaction mixtures used for the transformations studied here. Tan and Rankin noted that in syntheses of mesoporous silica spheres, variations in the dielectric constant of the solvent alter the micelle organization and particle

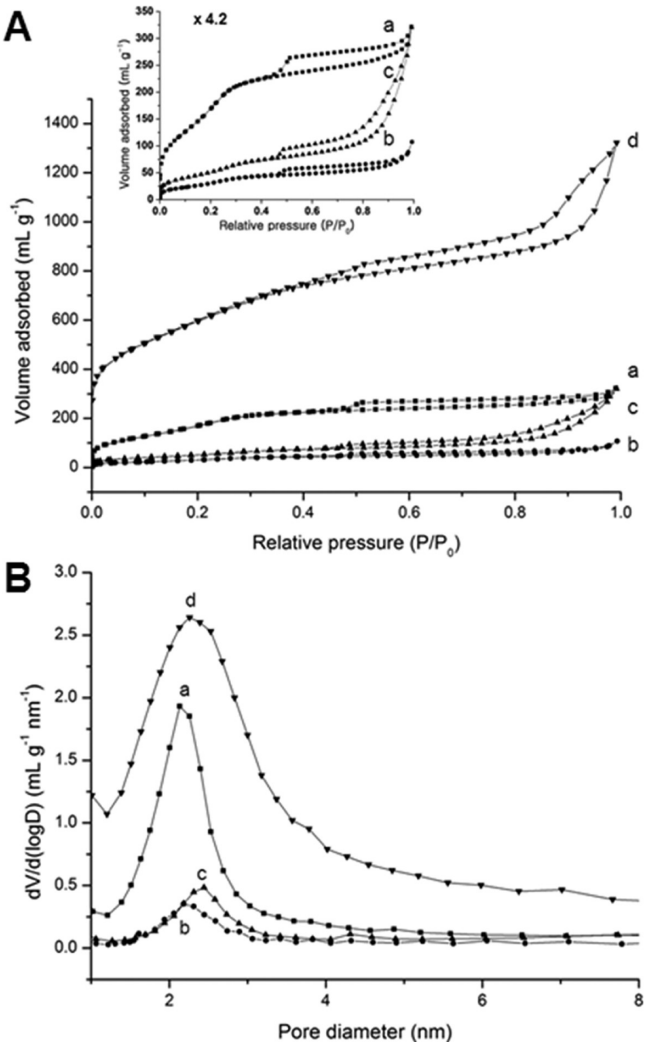


**Figure 6.** (A) Nitrogen sorption isotherms and (B) pore size distributions calculated from the adsorption branches by the BJH (Barrett–Joyner–Halenda) method. (a) HT-$SiO_2$-EtOH, (b) HT-$SiO_2$-*i*PrOH, (c) HT-$SiO_2$-BuOH, and (d) PFC-*i*PrOH.

morphology.[38] However, in our study, the procedures and reaction conditions were identical during hydrothermal treatment of all three sets of silica spheres. Furthermore, micelle formation was decoupled from the solvent used during the synthesis of the amorphous parent silica spheres. It is therefore reasonable to propose that the solvent employed during the Stöber sphere synthesis influenced the final morphology, most likely by controlling the extent of silica condensation. In their original report, Stöber and co-workers found that the condensation rates and sphere sizes depended on the type of alcohol used in the synthesis.[23] Reaction rates were fastest with methanol and slowest with *n*-butanol, and final particle sizes varied inversely with the rates. Artaki et al. investigated the role of nonalcoholic solvents during condensation of sol–gel silica, pointing out that a reduction in the rate of hydrolysis and condensation causes the formation of branched gel networks with increased porosity and reduced density.[39]

We employed $^{29}$Si solid-state MAS NMR spectroscopy of the parent silica spheres to investigate the degree of silica condensation in spheres prepared in the three different alcohols. The spectra of all parent silica spheres show two major peaks at −108 ppm and −98 ppm, with a small shoulder for the $SiO_2$-BuOH


dx.doi.org/10.1021/cm102829m |*Chem. Mater.* 2011, 23, 1761–1767

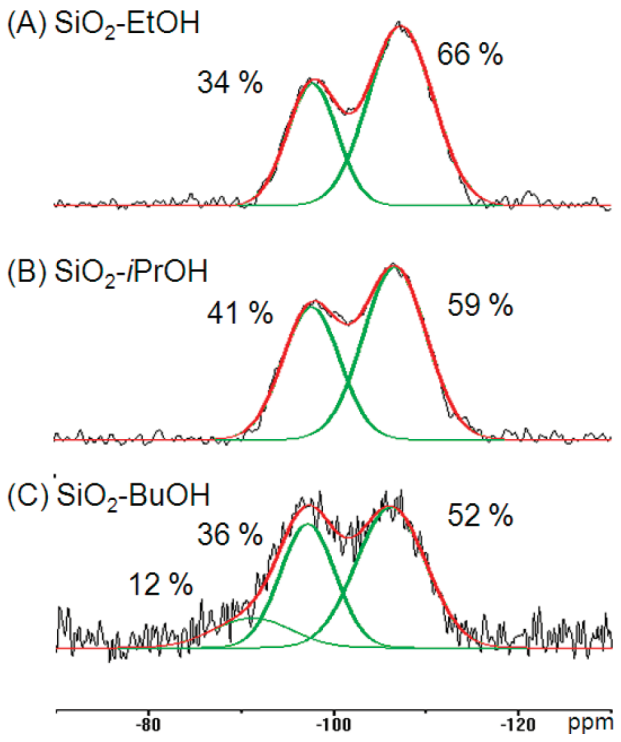


**Figure 7.** $^{29}$Si solid-state MAS NMR spectra of the parent silica spheres: (A) $SiO_2$-EtOH, (B) $SiO_2$-*i*PrOH, and (C) $SiO_2$-BuOH.

spheres at −89 ppm (Figure 7). These correspond to $Q^4$, $Q^3$, and $Q^2$ resonances, respectively, that is, a central Si with 4, 3, or 2 adjacent −O−Si− bridges and 0, 1, or 2 hydroxyl groups. The extent of condensation was estimated from the integrated peak areas by curve resolution of the $Q^3$ and $Q^4$ resonances. The amount of cross-linking was highest for $SiO_2$-EtOH spheres ($Q^3$ = 32−34%, $Q^4$ = 66−68%) and progressively lower for $SiO_2$-*i*PrOH ($Q^3$ = 40−41%, $Q^4$ = 59−60%) and $SiO_2$-BuOH spheres ($Q^2$= 12−13%, $Q^3$ = 33−36%, $Q^4$ = 52−54%). These ranges correspond to multiple samples prepared in separate batches (see also Supporting Information, Figure S3). Many factors may be responsible for the different degrees of condensation in different solvents, but in general, higher molecular weight alcohols retard the rate of hydrolysis and condensation of silica spheres.[23] Our NMR data show that this effect is small for the solvents used here, but the diverse surface morphologies reveal that such small differences in the silica connectivity can significantly affect the reactivity of the spheres under specific conditions.

During the pseudomorphic transformation reaction, partial dissolution of silica by the alkaline solution occurs simultaneously with the assembly of the surfactant. The small differences in the extent of silica sphere condensation caused by the original solvents thus could result in different dissolution rates of silica structures during the hydrothermal reaction, which would alter the ratio between reactive silica oligomers and surfactant molecules. The more highly condensed $SiO_2$-EtOH spheres dissolved to a lesser extent. Therefore, less dissolved silica was available for redeposition, resulting in the smallest increase in average sphere diameter. For these spheres, the transformation to mesoporous spheres was largely pseudomorphic as described in previous studies.[24] Relatively less condensed and more reactive silica spheres ($SiO_2$-*i*PrOH and $SiO_2$-BuOH) produced more pitted mesoporous shells that surrounded nonporous cores. In these cases it appears that silica had dissolved to a greater degree and then redeposited on nondissolved spheres. Surfactant molecules were associated more strongly with the shell structure and were not readily available to penetrate the core. Hence, for these two sphere systems, the hydrothermal transformations may not have been truly pseudomorphic with respect to individual particles, but for the overall samples, spherical shapes were still maintained after additional pores were introduced. The core−shell morphology was most pronounced with the following optimized molar ratio of reagents 1 $SiO_2$: 0.18 CTAB: 0.44 NaOH: 750 $H_2O$: 75 EtOH. When only half this sodium hydroxide concentration was used to decrease the rate of dissolution, no significant morphological changes were observed for HT-$SiO_2$-*i*PrOH and HT-$SiO_2$-BuOH. On the other hand, when twice the concentration of sodium hydroxide was used, corrugated surfaces were also observed, but spheres tended to coalesce into irregular aggregates (see Supporting Information, Figure S4). We therefore conclude that the solvent used in the original sphere synthesis determines the degree of silica condensation, which affects the silica dissolution rate that determines the precursor:template ratio, the reaction depth relative to the sphere surface, and the redeposition processes during the pseudomorphic transformation. Specifically, the most highly condensed silica spheres were converted into mesoporous products in which uniform mesopores, templated by the cationic surfactant, permeated the spheres completely. As the degree of condensation in the parent spheres was systematically decreased, following the trend EtOH > *i*PrOH > BuOH for the solvent employed in the parent sphere synthesis, product spheres obtained after hydrothermal treatment progressively increased in size and built up a porous surface layer whose thickness increased in the order EtOH < *i*PrOH < BuOH. Whereas the diameters of surfactant-templated mesopores remained relatively constant for the three solvent systems (2.1−2.4 nm), the diameters of the larger secondary cavities in the surface layers increased in the order *i*PrOH < BuOH.

## 5. CONCLUSIONS

This study showed that the solvent used to prepare submicrometer silica spheres by Stöber syntheses affects the reactivity of the spheres in hydrothermal transformations that target mesoporous products. $^{29}$Si solid-state MAS spectroscopy revealed small differences in the extent of silica of condensation, depending on the solvent used for the preparation of amorphous silica spheres ($SiO_2$-EtOH, $SiO_2$-*i*PrOH or $SiO_2$-BuOH). The extent of condensation decreased systematically as the number of carbon atoms in the alcohol increased from EtOH to *i*PrOH to BuOH. These small differences caused significant morphological changes on the surface after hydrothermal reactions in the presence of a cationic surfactant within a specific range of conditions. Spheres prepared in EtOH had smooth surfaces and were mesoporous throughout. In this case the transformation can be considered largely pseudomorphic. Spheres synthesized in *i*PrOH or BuOH, solvents that retard condensation of silica, possessed progressively less interconnected silica networks. After hydrothermal transformations, the amorphous silica spheres were converted to solid core-mesoporous shell structures with narrow mesopore size distributions (diameters between 2.1−2.4 nm) but visible surface texture and cavities on the length scale of tens of nanometers. The openings of these cavities increased in average dimensions for spheres originally prepared in BuOH compared to those prepared in *i*PrOH. The kinetically

controlled dissolution and reassembly phenomena that influence the hydrothermal transformation provide approaches for synthesizing mesoporous structures with porous shells and dense cores from monodisperse amorphous silica spheres with well-controlled size. Such spheres with density gradients can be used as templates for nanocasting of hollow carbon spheres with mesoporous shells and surface features similar to those of the hydrothermal mesoporous silica products. An understanding of factors influencing the texture and surface morphology of uniform silica spheres and hollow carbon spheres is important in the development of these materials for chromatography, controlled release and other applications.

## ■ ASSOCIATED CONTENT

**Supporting Information.** Nitrogen sorption data of amorphous parent silica spheres produced in the different solvents, TEM images of nanocast hollow carbon spheres (PFC-EtOH) after HF etching, $^{29}$Si solid-state MAS NMR spectra of another batch of parent silica spheres, and SEM images of HT-$SiO_2$-*i*PrOH spheres synthesized using half or twice the regular NaOH concentration. This material is available free of charge via the Internet at http://pubs.acs.org.

## ■ AUTHOR INFORMATION

### Corresponding Author

*Fax: (+1) 612-626-7541. E-mail: a-stein@umn.edu. Homepage: www.chem.umn.edu/groups/stein.

## ■ ACKNOWLEDGMENT

This work was funded by the U.S. Department of Energy (DE-FG02-06ER46348) using resources at the Institute of Technology Characterization Facility, University of Minnesota, which receives partial support from NSF through the NNIN program and the MRSEC program of the NSF (DMR-0212302). We thank Professor G. Veglia and Dr. N. Traaseth for obtaining the $^{29}$Si MAS NMR spectra at the University of Minnesota Nuclear Magnetic Resonance Facility.

## ■ REFERENCES

(1) Chen, H.-T.; Huh, S.; Wiench, J. W.; Pruski, M.; Lin, V. S.-Y. *J. Am. Chem. Soc.* **2005**, *127*, 13305–13311.
(2) Shokouhimehr, M.; Piao, Y.; Kim, J.; Jang, Y.; Hyeon, T. *Angew. Chem., Int. Ed.* **2007**, *46*, 7039–7043.
(3) Zhang, Q.; Lee, I.; Ge, J.; Zaera, F.; Yin, Y. *Adv. Funct. Mater.* **2010**, *20*, 2201–2214.
(4) Lai, C.-Y.; Trewyn, B. G.; Jeftinija, D. M.; Jeftinija, K.; Xu, S.; Jeftinija, S.; Lin, V. S.-Y. *J. Am. Chem. Soc.* **2003**, *125*, 4451–4459.
(5) Lu, J.; Liong, M.; Zink, J. I.; Tamanoi, F. *Small* **2007**, *3*, 1341–1346.
(6) Zhu, Y.; Shi, J.; Shen, W.; Dong, X.; Feng, J.; Ruan, M.; Li, Y. *Angew. Chem., Int. Ed.* **2005**, *44*, 5083–5087.
(7) Kirkland, J. J.; Truszkowski, F. A.; Dilks, C. H.; Engel, G. S. *J. Chromatogr., A* **2000**, *890*, 3–13.
(8) Martin, T.; Galarneau, A.; Renzo, F. D.; Brunel, D.; Fajula, F.; Heinisch, S.; Crétier, G.; Rocca, J.-L. *Chem. Mater.* **2004**, *16*, 1725–1731.
(9) Han, Y.; Lee, S. S.; Ying, J. Y. *Chem. Mater.* **2007**, *19*, 2292–2298.
(10) Grün, M.; Lauer, I.; Unger, K. K. *Adv. Mater.* **1997**, *9*, 254–257.
(11) Büchel, G.; Unger, K. K.; Matsumoto, A.; Tsutsumi, K. *Adv. Mater.* **1998**, *10*, 1036–1038.
(12) Nooney, R. I.; Thirunavukkarasu, D.; Chen, Y.; Josephs, R.; Ostafin, A. E. *Chem. Mater.* **2002**, *14*, 4721–4728.
(13) Wang, Y.; Caruso, F. *Chem. Mater.* **2005**, *17*, 953–961.
(14) Wang, Y.; Caruso, F. *Adv. Mater.* **2006**, *18*, 795–800.
(15) Wang, Y.; Yu, A.; Caruso, F. *Angew. Chem., Int. Ed.* **2005**, *44*, 2888–2892.
(16) Lu, Y.; Fan, H.; Stump, A.; Ward, T. L.; Rieker, T.; Brinker, C. J. *Nature* **1999**, *398*, 223–226.
(17) Grün, M.; Unger, K. K.; Matsumoto, A.; Tsutsumi, K. *Microporous Mesoporous Mater.* **1999**, *27*, 207–216.
(18) Yoon, S. B.; Sohn, K.; Kim, J. Y.; Shin, C.-H.; Yu, J.-S.; Hyeon, T. *Adv. Mater.* **2002**, *14*, 19–21.
(19) Tan, B.; Lehmler, H.-J.; Vyas, S. M.; Knutson, B. L.; Rankin, S. E. *Adv. Mater.* **2005**, *17*, 2368–2371.
(20) Chen, H.; Hu, T.; Zhang, X.; Huo, K.; Chu, P. K.; He, J. *Langmuir* **2010**, *26*, 13556–13563.
(21) Ganguly, A.; Ahmad, T.; Ganguli, A. K. *Langmuir* **2010**, *26*, 14901–14908.
(22) Kim, T.-W.; Chung, P.-W.; Lin, V. S.-Y. *Chem. Mater.* **2010**, *22*, 5093–5104.
(23) Stöber, W.; Fink, A.; Bohn, E. *J. Colloid Interface Sci.* **1968**, *26*, 62–69.
(24) Martin, T.; Galarneau, A.; Renzo, F. D.; Fajula, F.; Plee, D. *Angew. Chem., Int. Ed.* **2002**, *41*, 2590–2592.
(25) Botella, P.; Corma, A.; Navarro, M. T. *Chem. Mater.* **2007**, *19*, 1979–1983.
(26) Galarneau, A.; Iapichella, J.; Bonhomme, K.; Renzo, F. D.; Kooyman, P.; Terasaki, O.; Fajula, F. *Adv. Funct. Mater.* **2006**, *16*, 1657–1667.
(27) Lim, S.; Ranade, A.; Du, G.; Pfefferle, L. D.; Haller, G. L. *Chem. Mater.* **2006**, *18*, 5584–5590.
(28) Lee, J.; Sohn, K.; Hyeon, T. *J. Am. Chem. Soc.* **2001**, *123*, 5146–5147.
(29) Wang, Z.; Li, F.; Ergang, N. S.; Stein, A. *Chem. Mater.* **2006**, *18*, 5543–5553.
(30) Kim, J. H.; Yoon, S. B.; Kim, J.-Y.; Chae, Y. B.; Yu, J.-S. *Colloids Surf., A* **2008**, *313−314*, 77–81.
(31) Pauwels, B.; Tendeloo, G. V.; Thoelen, C.; Rhijn, W. V.; Jacobs, P. A. *Adv. Mater.* **2001**, *13*, 1317–1320.
(32) Möller, K.; Kobler, J.; Bein, T. *Adv. Funct. Mater.* **2007**, *17*, 605–612.
(33) Lu, A.-H.; Schüth, F. *C. R. Chim.* **2005**, *8*, 609–620.
(34) Yang, H.; Zhao, D. *J. Mater. Chem.* **2005**, *15*, 1217–1231.
(35) Yoon, S. B.; Kim, J.-Y.; Kim, J. H.; Park, Y. J.; Yoon, K. R.; Park, S.-K.; Yu, J.-S. *J. Mater. Chem.* **2007**, *17*, 1758–1761.
(36) Deng, Y.; Qi, D.; Deng, C.; Zhang, X.; Zhao, D. *J. Am. Chem. Soc.* **2008**, *130*, 28–29.
(37) Tendeloo, G. V.; Lebedev, O. I.; Collart, O.; Cool, P.; Vansant, E. F. *J. Phys.:Condens. Matter* **2003**, *15*, S3037–S3046.
(38) Tan, B.; Rankin, S. E. *J. Phys. Chem. B* **2004**, *108*, 20122–20129.
(39) Artaki, I.; Zerda, T. W.; Jonas, J. *J. Non-Cryst. Solids* **1986**, *81*, 381–395.